PSFC/JA-08-44

State Reconstruction and Noise Reduction by Kalman Filter in the Vertical Position Control on Alcator C-Mod

M. FERRARA*, I.H. HUTCHINSON, S.M. WOLFE

M.I.T. Plasma Science and Fusion Center

190 Albany Street, Cambridge, 02139 MA

February 25, 2009

Total number of pages: 43.

Total number of figures: 13.

*Corresponding author: mferrara@mit.edu

Title: State Reconstruction and Noise Reduction by Kalman Filter in the Vertical Position Control on Alcator C-Mod

Authors: M. FERRARA, I.H. HUTCHINSON, S.M. WOLFE

Abstract

The main sources of noise and pick-ups in Alcator C-Mod are identified and their effects on the measurement and control of the vertical position are evaluated. Broadband noise may affect controllability of C-Mod plasmas at limit elongations and may become an issue with high-order controllers, therefore two applications of Kalman filters are investigated. A Kalman filter is compared to a state observer based on the pseudo-inverse of the measurement matrix and proves to be a better candidate for state reconstruction for vertical stabilization, provided adequate models of the system, the inputs, the process and measurement noise and an adequate set of diagnostic measurements are available. A single-input single-output application of the filter for the vertical observer rejects high frequency noise without destabilizing high-elongation plasmas.

Keywords: measurement noise, vertical control, Kalman filter. PACS: 52.55.-s

1 Introduction

Plasmas with shaped cross-sections have higher MHD stability limits [1], but require sophisticated feedback control [2], [3]. Moreover, vertically elongated plasmas are vertically unstable and require feedback stabilization [4], [5], [6], [7], [8], [9].

Noise enters the feedback control loop at various points and limits measurement resolution and control precision. A general evaluation of noise in tokamak machines is not possible, because noise is very dependent on the specific hardware, its operating conditions and its surrounding environment. However, a collection of data from existing machines may help to predict noise contributions and their implications in large-scale reactors. In section 2 we discuss the main sources of broadband noise and sinusoidal pick-ups in Alcator C-Mod and their effects on the measurement and control of the vertical position.

Other forms of perturbations originating from the physics of tokamak plasmas are generally referred to as disturbances: they can be step-wise perturbations, such as beta drops, large injections, etc., or periodic perturbations, such as tearing modes. The loop response to noise and disturbances can be optimized by assigning the poles of the closed-loop system with full-state feedback control [10]. Full-state feedback control has also been proposed for the ITER vertical stabilization loop [11]. The first stage of a full-state controller is a state observer which uses a-priori knowledge and real time

observations to reconstruct the states of the system. A widely used state observer is the Kalman filter [12]. Other groups have shown that a Kalman filter is effective at discriminating Resistive Wall Modes from noise and interferences [13], [14]. In section 3 we discuss the design of a Kalman filter to reconstruct the states relevant for plasma vertical stabilization. In section 4 we illustrate a single-input single-output application of the filter to reject noise from the vertical observer and improve plasma controllability at limit elongations.

2 Measurement of Noise and Pick-ups in Alcator C-Mod

Figure 1 shows the configuration of the Alcator C-Mod vertical control system along with the main sources of noise and pick-up[1]. The axisymmetric coils OH1, OH2U, OH2L are used for inductive current drive and for vertical position control, while EF1U, EF1L, EF2U, EF2L, EF3, EF4 are used for plasma shape and position control. The anti-series EFC coils are used for vertical stabilization and are driven by a fast chopper power supply.

Noise sources are indicated in red: the current noise of the power supplies, the measurement noise of the magnetic diagnostics and the plasma noise. The magnetic diagnostics in C-Mod consists of a large set of flux loops and

[1]In the following, noise is used for broadband gaussian processes, while pick-up is used for narrowband interferences. Plasma noise is used to indicate spurious signals arising from the plasma itself, which are considered to be broadband and gaussian.

magnetic field probes. Pick-ups are indicated in blue: the alternator and line frequency at the power supplies and the line frequency in the magnetic diagnostics. The chopper bang-bang behavior is mostly negligible because of its high frequency[2].

The vertical position is reconstructed from magnetic measurements through a well validated linear observer [2], whose output is the product of the vertical position of the current centroid and the plasma current (*ZCUR Observer* in figure 1). A first feedback loop *PID Slow*, with proportional, derivative and integral gains, controls the vertical position on the time scale of the poloidal equilibrium (i.e. fractions of a second); the output of the PID controller generates a demand to all of the equilibrium field power supplies with the vector of coefficients *Slow Z Controller*. A second loop *PD Fast*, with proportional and derivative gains, stabilizes the vertical position on the time scale of the vertical instability (i.e. milliseconds); the output of the PD controller drives only the chopper with the gain *Fast Z Controller*. The chopper is connected to the anti-series EFC coil pair, which is the actuator for vertical stabilization. The bandwidth of the fast loop is cut off at $800Hz$ by a 4-th order Butterworth filter at the input of the chopper.

The noise and pick-up of the magnetic diagnostics were estimated from open-loop tests with no power supplies and no plasma. The typical $60Hz$ pick-up is $\sim 2mV$ and the broadband contribution is $\sim 2.3mV$ on each

[2]The chopping frequency at zero input demand is $\sim 3.5kHz$. In standard operation conditions, this frequency does not move down into the band of interest, even during large input modulation.

channel (RMS values). In physical units, the latter figure is equivalent to $\sim 1.2mWb$ on the flux loops and $\sim 1.2mT$ on the magnetic field probes. The total pick-up on the vertical observer is $\sim 13mV$ and the broadband contribution is approximately the same value $\sim 13mV$. In physical units, $13mV \equiv 0.3mm\ MA$.

The current noise in the control coils was estimated from power supply test shots at constant demand. The signals produced in the magnetic diagnostics by current fluctuations can exceed the diagnostics noise in a few specific channels, but the overall effect on the vertical observer is negligible.

The output of three of the power supplies show significant pick-up at frequencies of $60Hz$ and $54Hz$[3] and harmonics. The direct coupling of the pick-ups with the vertical observer is negligible, however they do limit the performance of C-Mod by driving large vertical oscillations of high-elongation plasmas.

2.1 Effects of Noise and Pick-ups on the Vertical Position

Figure 2 shows the spectra of the vertical position observer (ZCUR) for different target plasmas[4]. The spectral analysis is conducted on samples taken during $0.5s$ of the flattop with an interval $T = 100\mu s$, the spectral

[3] In Alcator C-Mod some of the equilibrium field supplies are powered directly from the grid, others are powered through an alternator whose operating frequency varies from $\sim 57Hz$ to $\sim 54Hz$ during a plasma discharge.

[4] In the following κ refers to the elongation at the separatrix.

resolution is $\Delta f = 2Hz$. Most of the information is at low frequency $0 - 200Hz$. The main features in these spectra are the components at $\sim 54Hz$ and harmonics ($\sim 108Hz$, $\sim 162Hz$) and $60Hz$ and harmonics ($120Hz$, $180Hz$), corresponding to real plasma oscillations driven by the pick-ups on some of the power supplies, and the closed loop resonances at $\sim 20Hz$ and $\sim 110Hz$[5]. Independent X-ray emission measurements show that their amplitude can be several millimeters in high-elongation shots.

For a typical elongation $\kappa = 1.7$, the total broadband noise is $\sigma_{ZCUR} \sim 1mm\ MA$, resulting from the magnetic diagnostics noise, the plasma noise and the effects of the current noise in the control coils. The diagnostics noise amounts to $\sigma_{Diag} \sim 0.3mm\ MA$, while the effects of the current noise are mostly negligible, therefore the plasma contributes most of the broadband noise in the vertical observer:

$$\sigma_{Plasma} = \sqrt{\sigma^2_{ZCUR} - \sigma^2_{Diag}} \lesssim 1mm\ MA \tag{1}$$

Finally, vertical stabilization uses derivative feedback: it is therefore useful to estimate the broadband noise affecting the measurement of the vertical velocity of the plasma (velocity resolution), which on C-Mod is $\sigma_{dZCUR/dt} \sim 1m/s\ MA$, in the $800Hz$ bandwidth of the fast vertical channel. Higher-order derivatives would amplify the high frequency noise and further

[5] The vertical position feedback loop has two resonances, at $\sim 20Hz$ and $\sim 110Hz$. The former mode is coupled with the slow poloidal equilibrium, while the latter corresponds to the fast vertical stabilization system. With the nominal control gains the "slow mode" is mostly suppressed.

reduce the control precision.

3 State Observer for Vertical Stabilization Based on a Kalman Filter

A Kalman filter uses a-priori knowledge of the system and of noise processes and available observations to reconstruct the states of the system. A linear dynamic model of the plasma vertical position is obtained by discretizing the axisymmetric structures of the tokamak in toroidal elements, or circuits, each one with a specific resistance, self-inductance and mutual inductances, and by writing the coupled circuit equations inclusive of plasma mediated effects [15]. A distinction is made between active elements, which are fed by external voltages, and passive elements. The final result is a state-space system of the form:

$$\frac{d\left(\delta \mathbf{I}_{cv}\right)}{dt} = \mathbf{A}\delta \mathbf{I}_{cv} + \mathbf{B}\delta \mathbf{V}_c \tag{2}$$

where $\delta \mathbf{I}_{cv} \equiv [\delta \mathbf{I}_c; \delta \mathbf{I}_v]$ is the vector of perturbations of active and passive currents respectively and $\delta \mathbf{V}_c$ is the vector of external voltages (its coefficients are zero for passive elements). In the case of C-Mod, the problem of vertical stability is well approximated by a single-input multiple-output (SIMO) system, which evolves on a time-scale much faster than the poloidal equilibrium. The SIMO's input is δV_{vs}, i.e. the demand to the vertical stabilization EFC

coils. The state equation is obtained by setting all the inputs to zero, except for δV_{vs}.

$$\frac{d\left(\delta \mathbf{I}_{cv}\right)}{dt} = \mathbf{A}\delta \mathbf{I}_{cv} + \mathbf{b}\delta V_{vs} \tag{3}$$

Note that the matrix $\mathbf{B}$ is now a vector $\mathbf{b}$. The SIMO's output is the vector of diagnostic measurements $\delta \mathbf{y}$, comprising the flux loops, the poloidal field coils, the Rogowski coil and the control currents:

$$\delta \mathbf{y} = \mathbf{C}\delta \mathbf{I}_{cv} \tag{4}$$

Our full state-space model of tokamak and plasma is of order 200 and needs to be reduced for real-time computation of the filter. In our custom implementation of model reduction, the plant is firstly diagonalized and the eigenvalues ordered so that the unstable mode is in the lower right corner of the state matrix. The stable part of the plant is then reduced with Schur balanced truncation [18]. Finally, the system and the truncation matrices are augmented with the unstable mode and the reduced system is diagonalized, in order to preserve the identity of the modes. A high-elongation equilibrium with growth rate $\lambda = 370 rad/s$ is used here and in the following for numerical studies and simulations. The corresponding matrices are extracted from calibrated Alcasim simulations [16] of a high-elongation shot.

One problem is to determine how many modes are enough to reproduce the input-output response of the system. For this purpose, we introduce the

relative error bound:

$$\varepsilon \equiv \frac{2\sum_{i:excluded}\sigma_i}{\sum_{i:all}\sigma_i} \tag{5}$$

where the Hankel Singular Values (HSV's) σ_i measure the contribution of the modes of the system to the energy of the input-output response [17]. Figure 3 shows the relative error bound for model reduction of our reference equilibrium. Because the error plateaus above five modes, this number seems to be sufficient to reproduce the stable part of the system.

Figure 4 shows the eigenvalues of the reduced model for different orders N_{red}. This is a convenient way to understand which modes are kept in the reduced model. Blue diamonds show some of the stable eigenvalues for order $N_{red} = 9$. There are some slow modes with small negative eigenvalues, which are mainly localized in the equilibrium field coils. There is also the EFC mode, which is localized in the EFC coils and the nearest wall, and has a decay constant $\sim -200 rad/s$. The remaining modes have even smaller time constants. As the order is reduced to $N_{red} = 5$ (magenta circles), only two of the slow modes, the EFC mode and a couple of faster modes are kept, however the fastest mode at $\sim -2600 rad/s$ should be a result of the synthesis of the two fastest modes of $N_{red} = 9$. The identity of the modes at lower orders can be analyzed by similar arguments.

The tokamak and plasma's reduced state-space $\{\mathbf{A}_r, \mathbf{b}_r, \mathbf{C}_r\}$ is augmented with the vertical stabilization power supply's state-space $\{\mathbf{A}_{ps}, \mathbf{b}_{ps}, \mathbf{c}_{ps}\}$ to

obtain equations 6 and 7:

$$\frac{d\mathbf{x}}{dt} = \begin{bmatrix} \mathbf{A}_{ps} & \mathbf{0} \\ \mathbf{b}_r\mathbf{c}_{ps} & \mathbf{A}_r \end{bmatrix} \mathbf{x} + \begin{bmatrix} \mathbf{b}_{ps} \\ \mathbf{0} \end{bmatrix} u = \mathbf{A}_{tot}\mathbf{x} + \mathbf{b}_{tot}u \tag{6}$$

$$\delta\mathbf{y} = \begin{bmatrix} \mathbf{0} & \mathbf{C}_r \end{bmatrix} \mathbf{x} = \mathbf{C}_{tot}\mathbf{x} \tag{7}$$

where $\mathbf{x} \equiv [\mathbf{x}_{ps}; \delta\mathbf{I}_{cv}]$ is the augmented state vector, $\mathbf{x}_{ps}$ stands for the internal states of the supply and u is the power supply demand.

Finally, the model is discretized on the sampling time T of the C-Mod digital plasma control system, leading to equations 8 and 9:

$$\mathbf{x}(k) = \mathbf{A}_d\mathbf{x}(k-1) + \mathbf{b}_d u(k-1) + \mathbf{w}(k) \tag{8}$$

$$\mathbf{y}(k) = \mathbf{C}_d\mathbf{x}(k) + \mathbf{r}(k) \tag{9}$$

where $\mathbf{A}_d = \exp(\mathbf{A}_{tot}T)$, $\mathbf{b}_d = \int_0^T \exp(\mathbf{A}_{tot}\tau)\, d\tau \mathbf{b}_{tot}$, $\mathbf{C}_d = \mathbf{C}_{tot}$, $\mathbf{w}$ is the process noise and $\mathbf{r}$ is the measurement noise.

3.1 Kalman Filter Equations

A Kalman filter comprises a set of time-update equations (equations 10 and 11) and a set of measurement-update equations (equations 12 - 14) [12]:

$$\widehat{\mathbf{x}}^{-}(k) = \mathbf{A}_d \widehat{\mathbf{x}}(k-1) + \mathbf{b}_d u(k-1) \tag{10}$$

$$\mathbf{P}^{-}(k) = \mathbf{A}_d \mathbf{P}(k-1) \mathbf{A}_d^T + \mathbf{Q}\,(k) \tag{11}$$

$$\mathbf{K}(k) = \mathbf{P}^{-}(k) \mathbf{C}_d^T \left[\mathbf{C}_d \mathbf{P}^{-}(k) \mathbf{C}_d^T + \mathbf{R}\,(k) \right]^{-1} \tag{12}$$

$$\widehat{\mathbf{x}}(k) = \widehat{\mathbf{x}}^{-}(k) + \mathbf{K}(k) \left[\mathbf{y}_{\exp}(k) - \mathbf{C}_d \widehat{\mathbf{x}}^{-}(k) \right] \tag{13}$$

$$\mathbf{P}(k) = \left[\mathbf{I} - \mathbf{K}(k) \mathbf{C}_d \right] \mathbf{P}^{-}(k) \tag{14}$$

where $\widehat{\mathbf{x}}^{-}(k)$ is the a priori estimate of the state at time k; $\mathbf{P}(k)$ is the error covariance matrix at time k: $\mathbf{P}(k) \equiv E\left\{ \left(\delta\mathbf{x}\,(k) - E\left\{ \delta\mathbf{x}\,(k) \right\} \right)^T \cdot \left(\delta\mathbf{x}\,(k) - E\left\{ \delta\mathbf{x}\,(k) \right\} \right) \right\}$, $\delta\mathbf{x} \equiv \mathbf{x}(k) - \widehat{\mathbf{x}}(k)$ ($\mathbf{P}^{-}(k)$ is the corresponding a priori estimate); $\mathbf{Q}\,(k)$ is the process noise covariance matrix: $\mathbf{Q}\,(k) \equiv E\left\{ \left(\mathbf{w}\,(k) - E\left\{ \mathbf{w}\,(k) \right\} \right)^T \cdot \left(\mathbf{w}\,(k) - E\left\{ \mathbf{w}\,(k) \right\} \right) \right\}$; $\mathbf{K}(k)$ is the Kalman gain at time k; $\mathbf{R}$ is the measurement noise covariance matrix: $\mathbf{R}\,(k) \equiv E\left\{ \left(\mathbf{r}\,(k) - E\left\{ \mathbf{r}\,(k) \right\} \right)^T \cdot \left(\mathbf{r}\,(k) - E\left\{ \mathbf{r}\,(k) \right\} \right) \right\}$; $\mathbf{y}_{\exp}(k)$ is the output measurements at time k.

If the process and measurement noise are stationary ($\mathbf{Q}\,(k) \equiv \mathbf{Q}$, $\mathbf{R}\,(k) \equiv \mathbf{R}$), the Kalman gain and the error covariance matrix can be calculated off-line. The error covariance matrix is initialized to the process noise covariance matrix $\mathbf{P}(0) \equiv \mathbf{Q}$ and equations 11, 12, 14 are solved iteratively until con-

vergence. The only equations to compute in real time are 10 and 13, which can be written in compact form:

$$\widehat{\mathbf{x}}(k) = \mathbf{A}_d^{'}\widehat{\mathbf{x}}(k-1) + \mathbf{b}_d^{'}u(k-1) + \mathbf{K}\mathbf{y}_{\exp}(k) \tag{15}$$

where $\mathbf{A}_d^{'} = (\mathbf{I} - \mathbf{K}\mathbf{C}_d)\,\mathbf{A}_d$, $\mathbf{b}_d^{'} = (\mathbf{I} - \mathbf{K}\mathbf{C}_d)\,\mathbf{b}_d$.

The process covariance $\mathbf{Q}$ and the measurement covariance $\mathbf{R}$ are external parameters: their relative magnitude sets the trade-off between filter bandwidth and noise rejection. In the simplest case, the process covariance matrix $\mathbf{Q}$ is initialized assuming that the noise processes driving the modes of the reduced model are uncorrelated gaussian processes with uniform variance σ_w^2 and that the noise processes driving the internal states of the power supply have zero amplitude. The measurement covariance matrix $\mathbf{R}$ is initialized assuming that all the channels are uncorrelated gaussian processes with the same variance σ_R^2. The ratio σ_R^2/σ_w^2 is an external parameter available for tuning: when $\sigma_R^2/\sigma_w^2 \rightarrow 0$, the filter assumes that all the fluctuations of the measurements are a direct consequence of the fluctuations of the states and no filtering occurs. This is readily seen in the simple case when $\mathbf{C}_d$ is square and invertible. Solving equations 11, 12, 14 gives $\mathbf{K} = \mathbf{C}_d^{-1}$. Then, from equation 13, $\widehat{\mathbf{x}}(k) = \mathbf{C}_d^{-1}\mathbf{y}_{\exp}(k)$. Conversely, when $\sigma_R^2/\sigma_w^2 \rightarrow \infty$, the filter assumes that all the fluctuations of the measurements are noise and the measurements are discarded entirely. In fact, $\mathbf{K} = \mathbf{0}$ in this case.

For the purpose of simulations, a different paramenter is introduced $\alpha^2 \equiv$

$\frac{\|\mathbf{A}_{ZCUR}\|^2}{\|\mathbf{A}_{ZCUR}\mathbf{C}_d\|^2}\frac{\sigma_R^2}{\sigma_w^2}$, where $\mathbf{A}_{ZCUR}$ is the vector of coefficients of the vertical observer.

3.2 Simulated Behavior of the Filter

Figure 5 shows the linear model to test the behavior of the filter. The vertical stabilization loop comprises the full model of the plant, augmented with the dynamic models of the power supplies (*State-Space*); the linearized diagnostics (*Ctotalpc*); the digitizer (*Zero-Order Hold*), with the DPCS sampling time $T = 100\mu s$; the vertical observer (A_ZCUR), the fast PD controller (*Fast Controller*) and the chopper gain (*Chopper Gain*), which are the same as in experimental discharges.

The Kalman filter is implemented with a Matlab sFunction (*VerticalFilter6*).

A pseudo-inverse state observer (*pinv State-Observer*) is used to benchmark the behavior of the Kalman filter. The observer is preceded by an optimized low-pass filter (*Digital Filter Design*) in order to reject part of the measurement noise.

Process Noise is a vector of uncorrelated broadband gaussian noise processes of uniform amplitude, which is calibrated in order to produce RMS fluctuations of the vertical observer $\sim 0.5mm\ MA$ in the absence of all other noise sources.

Diagnostics Noise is a vector of uncorrelated broadband gaussian noise

processes of uniform amplitude, which is calibrated in order to obtain RMS fluctuations of the vertical observer $\sim 40mV$ in DPCS units, equivalent to the resolution of the vertical observer $\sim 1mm\ MA$. *60Hz Typical* is the $60Hz$ pick-up in the magnetic diagnostics of amplitude $2mV$ per channel.

$54Hz$ *Pick-up* models the large pick-up on OH2U and was calibrated in order to produce large $54Hz$ vertical oscillations of peak-to-peak amplitude $\sim 1.2cm$, as observed in experiments: it can be turned on or off to study how the filter behaves in the presence of broadband noise only or when a large sinusoidal input is present that is not included either in the SIMO model of the plant or in the model of noise in the Kalman filter.

The purpose of the linear model is to determine if the Kalman filter can reconstruct the states of a reduced-order system, while rejecting noise, better than a simple pseudo-inverse observer with an optimized low-pass filter, in realistic scenarios of noise and pick-ups. Moreover, the Kalman filter can be tested for robustness against parameter setting.

The pseudo-inverse observer is built by calculating the pseudo-inverse of the output matrix of the reduced-order system $\mathbf{C}_r$ with the Matlab *pinv* routine [19]. The observer does not reject most of the input noise, therefore it is necessary to add an optimized low-pass filter[6].

The error of the state observers is calculated by subtracting the recon-

[6]The filter was designed with the Digital Filter Design toolbox of Simulink, with the goal of rejecting most of the noise, without introducing enough phase lag to destabilize the feedback loop. The best solution appeared to be a 5-th order FIR Equiripple with $800Hz$ pass-band, $5kHz$ stop-band, $-40dB$ stop-band attenuation and phase lag < 10 deg at $200Hz$.

structed states from the real states, which are extracted from the full model with the truncation matrix *slbig*. The power spectrum is calculated for each one of the error signals and integrated in order to have both a spectral distribution and a RMS estimate of the error. The latter is normalized by the RMS values of the real states[7].

With the simple model of uniform process noise, the only knob available for tuning is the noise ratio α^2, which should be large enough to reject most of the measurement noise from the reconstructed states, without introducing significant distortion. In order to determine the optimal setting of this parameter, we inject a sine wave of appropriate frequency at the input of the plant, like *Test Sine* in figure 5. By looking at the Bode plots of this high-elongation equilibrium, we find that the phase margin is $\sim 7.4\,\mathrm{deg}$ at $100Hz$, which sets the maximum phase lag tolerable at this frequency, corresponding to $\alpha^2 \leq 4$.

The generalization to cases with non-uniform process fluctuations is possible by using a vector $\boldsymbol{\alpha}^2$ with components α_i^2 for the various (uncorrelated) modes.

In order to have a reference of how much error is tolerable, a simple argument can be made. The coefficients of the vector $\mathbf{c}_z \equiv \mathbf{A}_{ZCUR}\mathbf{C}_d$ represent the contribution of individual states to the vertical observer. The ratio of the

[7]The RMS values are only coarse zeroth-order estimates of the errors in state reconstruction, lumping together deterministic errors, such as amplitude and phase errors, and random fluctuations. A careful inspection of the time traces is always needed to separate these two cases.

vertical resolution σ_{ZCUR} and any coefficient of $\mathbf{c}_z$ represents an error that, by itself, would produce vertical fluctuations equal to the vertical resolution:

$$\sigma_{\varepsilon,i} = \sigma_{ZCUR} / \left| c_{z,i} \right| , \; i = 1, ...6 \tag{16}$$

If the state fluctuations are uncorrelated, then the state observer does not allow a more accurate representation of the vertical position than the C-Mod vertical observer if any of the errors is larger than the corresponding value $\sigma_{\varepsilon,i}$. In other words, the errors of all reconstructed states should be well below the corresponding $\sigma_{\varepsilon,i}$.

Figure 6 shows the superposition of real and reconstructed states with the pseudo-inverse observer and the Kalman filter. The $54Hz$ pick-up is initially off for a test with broadband gaussian noise only (consistent with the synthesis of the Kalman filter). Figure 7 shows the RMS values of the error signals together with "Max Error", i.e. the vector $\boldsymbol{\sigma}_\varepsilon$ normalized by the RMS values of the states.

All of the errors are well below the dashed line: both state observers allow a representation of the vertical position with lower noise than the standard C-Mod vertical observer, as it can be seen from direct inspection. However, in the case of the pseudo-inverse observer, this is due to the optimized low-pass filter at its input. In all the cases investigated the Kalman filter was consistently out-performing the pseudo-inverse observer, especially with non-uniform noise models.

Next, the $54Hz$ pick-up is introduced in simulations. Figures 8, 9 show results in this case. There are significant amplitude and phase errors in the reconstructed states by both the pseudo-inverse observer and the Kalman filter. In the latter case, a large set of values of $\boldsymbol{\alpha}^2$ was tried without significant improvements. This result is not surprising: the pseudo-inverse observer is the pseudo-inverse of the measurement matrix of a reduced-order model of the SIMO system, and therefore ignores the presence of a large additional input; similarly, the Kalman filter is simulating a reduced-order model of the SIMO plant; moreover, it assumes broadband gaussian noise only. In order to correctly reproduce the effects of the large pick-up a full MIMO formulation and a comprehensive model of noise and pick-ups are needed.

One important issue is how state reconstruction depends on the accuracy of the model of the plant. In order to answer this question, we tried two different simulations with broadband noise only:

1. the Kalman filter and the pseudo-inverse observer are built from an equilibrium with growth rate $\lambda = 314 rad/s$, about 15% smaller than the unstable eigenvalue of the plant;

2. the Kalman filter and the pseudo-inverse observer are built from an equilibrium with growth rate $\lambda = 282 rad/s$, about 24% smaller than the unstable eigenvalue of the plant.

In both cases the numbers are similar to those in figure 7, proving a robust behavior of the filter with respect to (small) errors in the model of the plant.

4 Model-based Filter for the Vertical Observer Based on a Kalman Filter

One special application of the Kalman filter looks at the Single-Input Single-Output (SISO) problem:

$$\frac{d\left(\delta \mathbf{I}_{cv}\right)}{dt} = \mathbf{A}\delta \mathbf{I}_{cv} + \mathbf{b}\delta V_{vs} \tag{17}$$

$$ZCUR = \mathbf{c}_z \delta \mathbf{I}_{cv} \tag{18}$$

where $ZCUR$ is the vertical position times the plasma current. Based on the predictions of the model in equations 17, 18, it is possible to design a filter for the vertical observer.

The procedure for model reduction, compounding and digitization are similar to those discussed for the SIMO system, with final result:

$$\mathbf{x}(k) = \mathbf{A}_d \mathbf{x}(k-1) + \mathbf{b}_d u(k-1) + \mathbf{w}\left(k\right) \tag{19}$$

$$ZCUR(k) = \mathbf{c}_{zd}\mathbf{x}(k) + r\left(k\right) \tag{20}$$

In the SISO case $\mathbf{R} \equiv \sigma_R^2 = \sigma_{ZCUR}^2 \sim \left(1mm\ MA\right)^2$ is readily available from the analysis of noise. Equation 15 becomes:

$$\widehat{\mathbf{x}}(k) = \mathbf{A}_d^{'}\widehat{\mathbf{x}}(k-1) + \mathbf{b}_d^{'}u(k-1) + \mathbf{k}ZCUR_{\exp}(k) \tag{21}$$

where the Kalman gain $\mathbf{k}$ is evaluated by solving equations 11, 12, 14 until convergence, and the output of the filter is given by:

$$ZCUR(k) = \mathbf{c}_{zd}\widehat{\mathbf{x}}(k) \tag{22}$$

The filter frequency response is obtained by calculating the z-transform [20] of equations 21 and 22:

$$\widehat{\mathbf{X}}(z) = \mathbf{A}_d^{'}\frac{\widehat{\mathbf{X}}(z)}{z} + \frac{\mathbf{b}_d^{'}}{z}U(z) + \mathbf{k}ZCUR_{\exp}(z) \tag{23}$$

$$\frac{ZCUR(z)}{ZCUR_{\exp}(z)} = \mathbf{c}_{zd}\left(z\mathbf{I} - \mathbf{A}_d^{'}\right)^{-1}\mathbf{b}_d^{'}\frac{U(z)}{ZCUR_{\exp}(z)} + z\mathbf{c}_{zd}\left(z\mathbf{I} - \mathbf{A}_d^{'}\right)^{-1}\mathbf{k} \tag{24}$$

$$F_{KF} = F_{SYS}F_{CTRL} + zF_K \tag{25}$$

where $F_{KF} \equiv ZCUR(z)/ZCUR_{\exp}(z)$, $F_{SYS} \equiv \mathbf{c}_{zd}\left(z\mathbf{I} - \mathbf{A}_d^{'}\right)^{-1}\mathbf{b}_d^{'}$, $F_{CTRL} \equiv U(z)/ZCUR_{\exp}(z)$, $F_K \equiv \mathbf{c}_{zd}\left(z\mathbf{I} - \mathbf{A}_d^{'}\right)^{-1}\mathbf{k}$.

F_{CTRL} is the transfer function of the PD controller in the vertical stabilization loop:

$$F_{CTRL} = m\left(\frac{D}{T}\frac{z-1}{z} + P\right) \tag{26}$$

where T is the sampling time and m is a scalar gain. The filter behavior is therefore affected by internal parameters, i.e. the noise ratio $\alpha^2 \equiv \frac{\sigma_R^2}{\|\mathbf{c}_{zd}\|^2 \sigma_w^2}$, and by external parameters, i.e. the controller gains P and D. By applying the transformation from z to s-domain, $z = \frac{2+sT}{2-sT}$, it is possible to draw the Bode plots for different parameter values.

Figure 10 shows the Bode plots of F_{KF} for different orders of the reduced model. When the order of the model is $N_{red} \geq 3$ the slow modes are included and the frequency response has a unitary DC gain, For $N_{red} \geq 6$ the frequency response is practically unchanged.

The broad minimum $\sim 60Hz$ and the broad maximum at $\sim 500Hz$ are caused by the combination of the terms in equation 25, i.e. the low-pass behavior of zF_K, the high pass behavior of F_{CTRL} and the cut-off of the chopper at $800Hz$. The location and width of these features change with the value of the derivative and proportional gains. Figure 11 shows the Bode plots of F_{KF} for $N_{red} = 6$, the nominal control gains $D = 6$, $P = 4$, and different values of the noise ratio.

The SISO Kalman filter was programmed in IDL and incorporated in the C-Mod Plasma Control System (PCS) as a real-time procedure on the vertical observer. It was initially tested with Alcasim simulations and off-line. Figure 12 shows the comparison of analytic and experimental transfer functions. At

the vertical signal frequency of approximately $120Hz$, the filter introduces a phase lead that actually improves the stability of the closed loop and an attenuation of approximately $-4dB$ that changes the dynamic behavior of the loop (the filter attenuation is equivalent to changing the control gains), but did not destabilize plasmas up to $\kappa = 1.84$. Figure 13 shows results from a shot where the filter was operating in the vertical stabilization loop.

It should be noted that in the SISO application of the Kalman filter only the measurement of the vertical position is used to correct the prediction of multiple states, therefore the problem is under-constrained and the internal states of the filter differ from the physical states of the plant: the main property of the filter of being an accurate state observer is not exploited. Moreover, as far as rejection of high-frequency noise, an optimized low-pass filter can do better than the SISO Kalman filter[8]. Therefore the SISO application of the Kalman filter is probably non-optimal.

5 Conclusions

The vertical resolution on C-Mod is $\sigma_{ZCUR} \sim 1mm\ MA$ and $\sigma_{dZCUR/dt} \sim 1m/s\ MA$, limited by broadband noise. The main contribution comes directly from the plasma, therefore it seems unlikely that significant noise reduction could be achieved by improving the diagnostic circuitry. On the

[8]For example, the 5-th order FIR Equiripple discussed in section 3.2 achieves $-40dB$ stop-band attenuation with phase lag < 10 deg at $200Hz$ and negligible amplitude distortion.

other hand, an optimized filter on the vertical observer may help reduce the broadband noise and improve plasma controllability at limit elongations $\kappa \sim 1.85$. At moderate elongations $\kappa \leq 1.80$, noise does not seems to be a major concern in C-Mod. However, if controllers with high-order derivatives were implemented, control precision might decrease because of higher noise levels: an accurate assessment of the trade-off between improvements of theoretical stability margins and loss of vertical resolution would then become necessary. We also discussed a larger perturbation, represented by the pick-ups at the output of the power supplies: this perturbation is particularly dangerous because it drives directly vertical oscillations of high-elongation plasmas, increases control power consumption and may cause loss of vertical control.

Noise rejection is important to minimize control power consumption and AC losses, especially in tokamaks with superconducting control coils. The loop response to noise and disturbances may be optimized through full-state feedback control. Our linear simulations prove that a Kalman filter performs better than our benchmark, a simple pseudo-inverse observer, in reconstructing the states of a system from available observations, provided adequate models of the system, the inputs and the process and measurement noise are available. The filter is particularly useful when measurement noise levels are at least comparable with process noise levels. We verified that omissions of small interferences in the model of noise in the filter, such as the $60Hz$ pick-up in the magnetic diagnostics, do not affect the filter's performance.

We also verified that small errors in the model of the plant do not reduce the filter's accuracy. However, omissions of large perturbations, such as the power supplies' pick-ups, cause unacceptable errors in the reconstruction of the states.

We also discussed a model-based filter for the vertical observer based on a SISO implementation of the Kalman filter. Simulations and experiments show that the filter rejects high-frequency noise without destabilizing high-elongation plasmas, however an optimized low-pass filter can achieve even stronger rejection of high-frequency noise.

References

[1] *Improved Magnetohydrodynamic Stability through Optimization of Higher Order Moments in Cross-section Shape of Tokamaks*, A.D. TURNBULL, Y.R. LIN-LIU, R.L. MILLER, T.S. TAYLOR, T.N. TODD. Phys. Plasmas 6, 1113 (1999).

[2] *Plasma Shape Control: a General Approach and its Application to Alcator C-Mod*, I.H. HUTCHINSON, S.F. HORNE, G. TINIOS, S.M. WOLFE, R.S. GRANETZ. Fusion Technology 30, 137 (1996).

[3] *A Framework for the Design of a Plasma Current and Shape Controller in Next-Generation Tokamaks*, M. ARIOLA, A. PIRONTI, A. PORTONE. Fusion Science and Technology 36, 263 (1999).

[4] *Control of the vertical instability in tokamaks*, E.A. LAZARUS, J.B. LISTER, G.H. NEILSON. Nucl. Fusion 30, 111 (1990).

[5] *Experimental study of the vertical stability of high decay index plasmas in the DIII-D tokamak*, J.B. LISTER, E.A. LAZARUS, A.G. KELLMAN *et al.*. Nucl. Fusion 30, 2349 (1990).

[6] *Stability of axisymmetric modes in JET*, M.R. PERRONE, J.A. WESSON. Nucl. Fusion 21, 871 (1981).

[7] *Feedback stabilization of the axisymmetric instability of a deformable tokamak plasma*, N. POMPHREY, S.C. JARDIN, D.J. WARD. Nucl. Fusion 29, 465 (1989).

[8] *Effects of plasma deformability on the feedback stabilization of axisymmetric modes in tokamak plasmas*, D.J. WARD, S.C. JARDIN. Nucl. Fusion 32, 973 (1992).

[9] *Axisymmetric Equilibrium and Stability Analysis in Alcator C-Mod, Including Effects of Current Profile, Measurement Noise and Power Supply Saturation*, M. FERRARA. Ph.D. Thesis, Massachusetts Institute of Technology, Cambridge (2009).

[10] *Control Systems Engineering* 4th ed., N.S. NISE. Wiley, Hoboken, NJ (2004).

[11] *ITER Control System Design and Assessment (CSD)*, Appendix E, 61 (2004).

[12] *Optimal Control and Estimation*, R.F. STENGEL. Dover Publications, New York, 342 (1994).

[13] *Model-based dynamic resistive wall mode identification and feedback control in the DIII-D tokamak*, Y. IN *et al.* Phys. Plasmas 13, 062512 (2006).

[14] *A Kalman Filter for Feedback Control of Rotating External Kink Instabilities in a Tokamak Plasma*, J.M. HANSON, R. JAMES, M.E. MAUEL, D.A. MAUER, G.A.

[15] *Valid Coordinate Systems for Linearized Plasma Shape Response Models in Tokamaks*, M.L. WALKER, D.A. HUMPHREYS. Fusion Science and Technology 50, 473 (2006).

[16] *Alcasim Axisymmetric Simulation Code for Alcator C-Mod*, M. FERRARA, I.H. HUTCHINSON, S.M. WOLFE, J.A. STILLERMAN, T.W. FREDIAN. In the Proceedings of the 45th IEEE Conference on Decision and Control, San Diego CA, December 2006.

[17] *Linear System Theory and Design (Oxford Series in Electrical and Computer Engineering)*, CHI-TSONG CHEN. Oxford University Press, USA, New York, 199 (1998).

[18] *A Schur Method for Balanced Model Reduction*, M.G. SAFONOV, R.Y. CHIANG. IEEE Trans. on Automat. Contr. 34, 729 (1989).

[19] URL www.mathworks.com/access/helpdesk/help/techdoc/ref/pinv.html

[20] *Discrete-Time Signal Processing* 2nd ed., A.V. OPPENHEIM, R.W. SCHAFER, J.R. BUCK. Prentice Hall (1999).

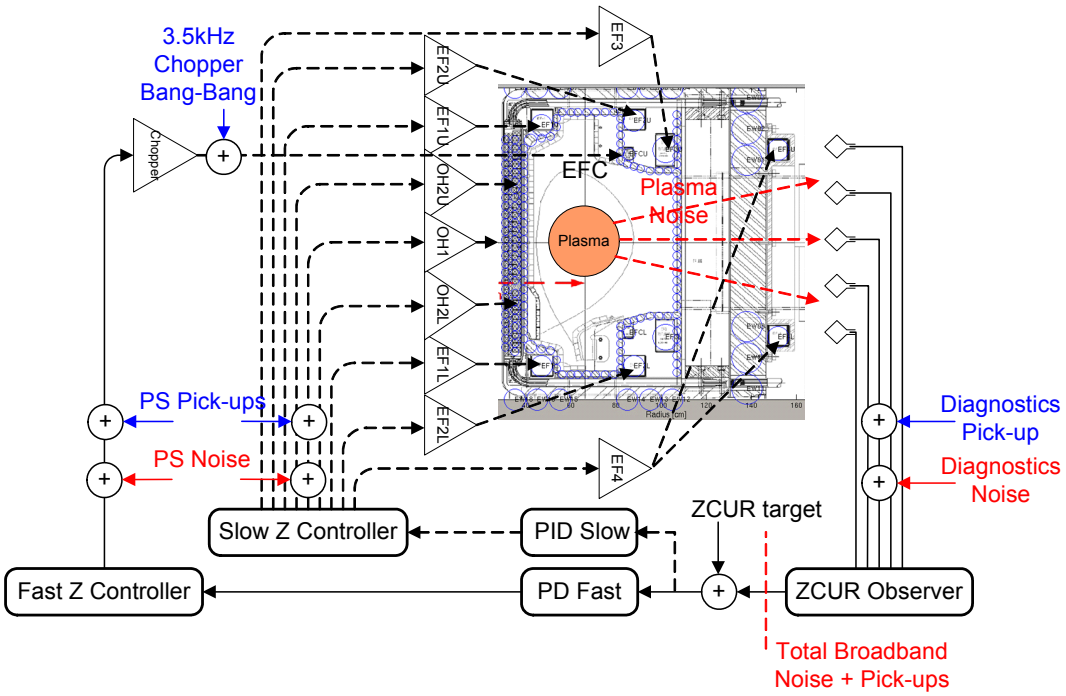

Figure 1: Sources of noise and pick-up in Alcator C-Mod.

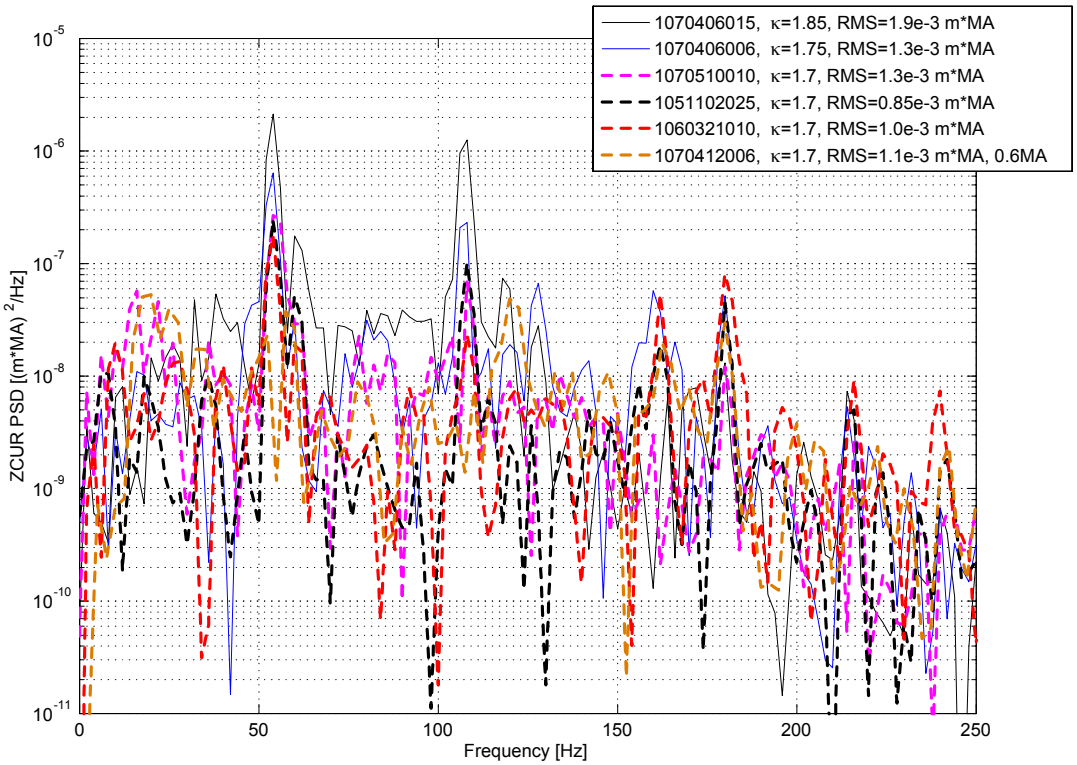

Figure 2: Comparison of the spectral power densities of ZCUR for different target plasmas. Power spectrum $< 0.1e-7$ for frequency $> 250Hz$.

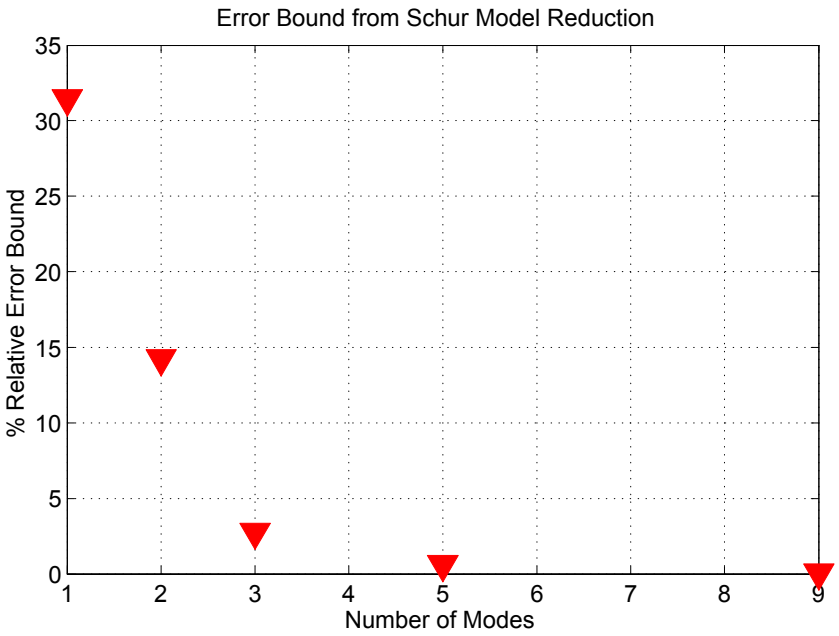

Figure 3: Error bound of the Schur balanced truncation of the stable part of a high-elongation equilibrium as a function of the number of modes retained in the model.

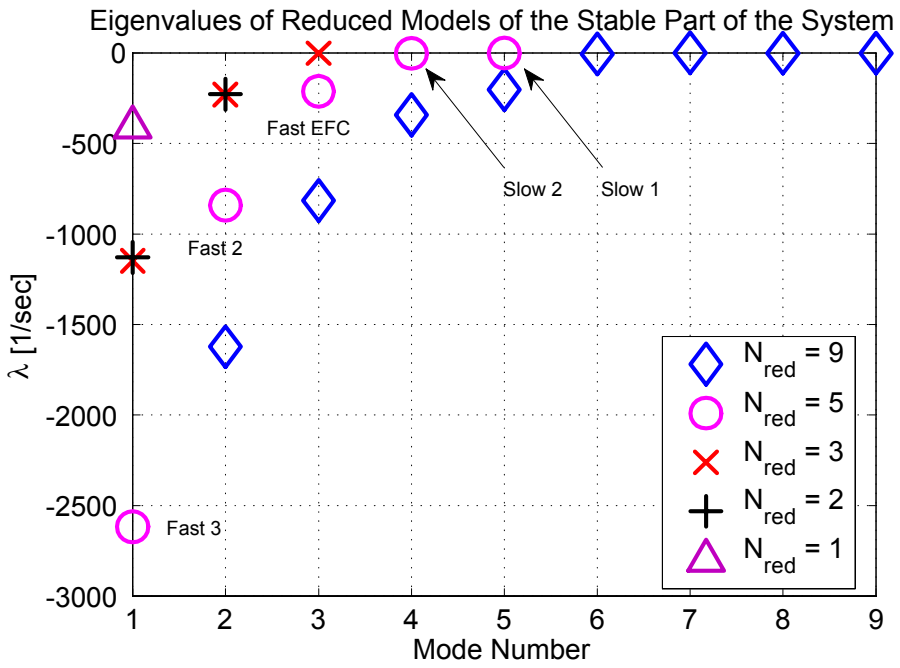

Figure 4: Eigenvalues of the reduced model of the stable part of the system for $N_{red} = 1, 2, 3, 5, 9$. The eigenvalues of the model of order 5 are labeled for future reference.

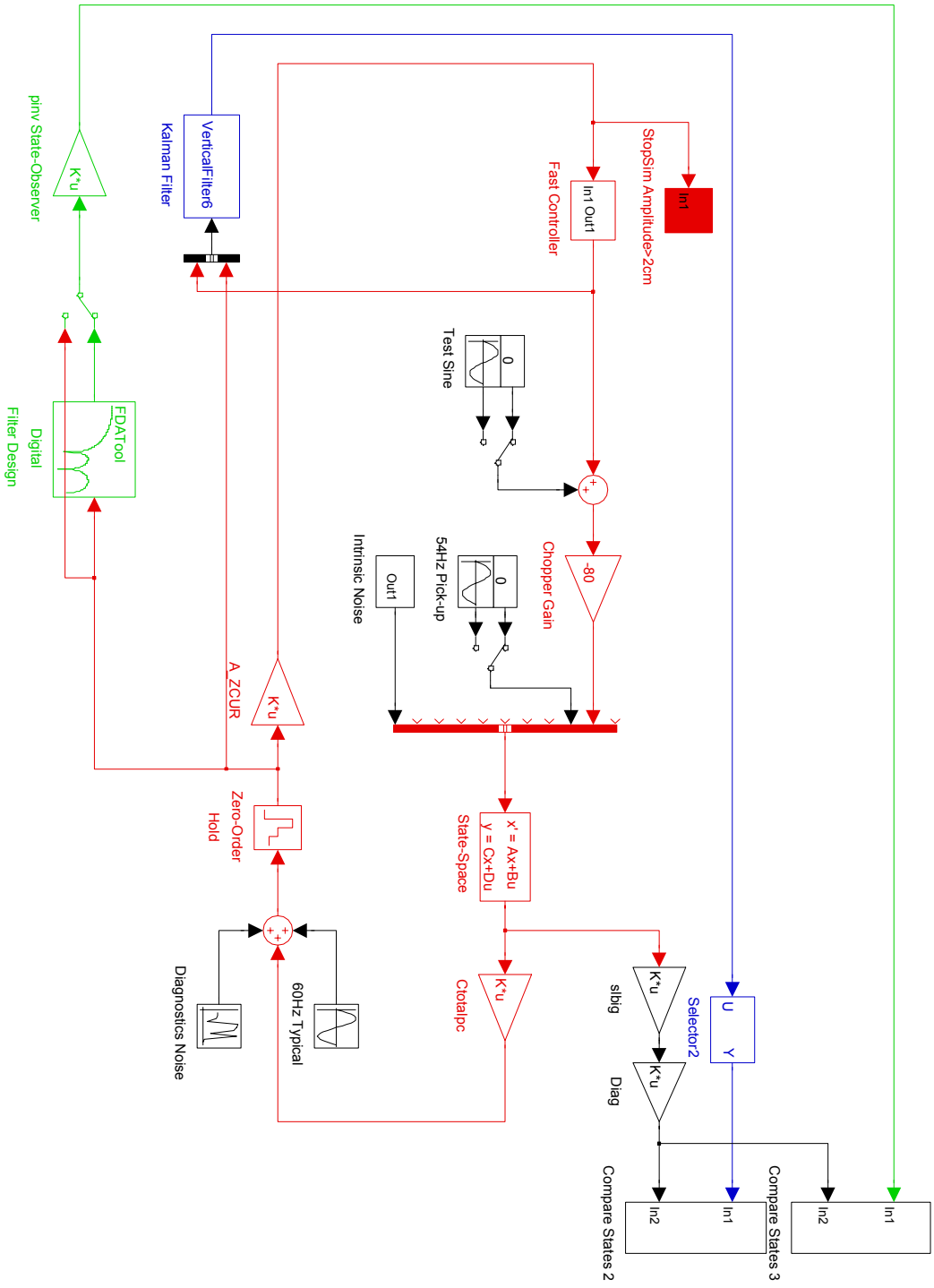

Figure 5: The linear model used to test the behavior of the Kalman filter.

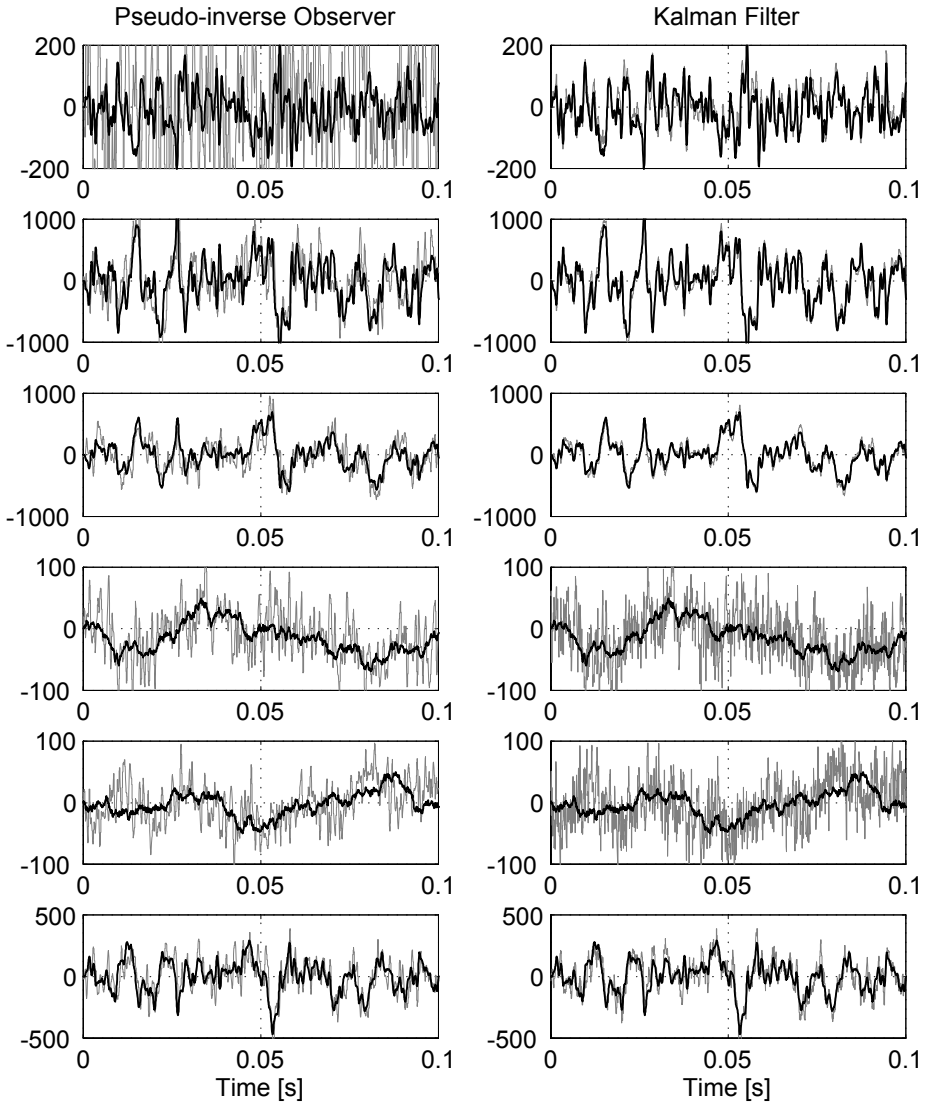

Figure 6: Comparison of real (black) and reconstructed states (light gray). Vertical axes are Amperes. The $54Hz$ pick-up is off. The process noise model is uniform with $\alpha^2 = 4$.

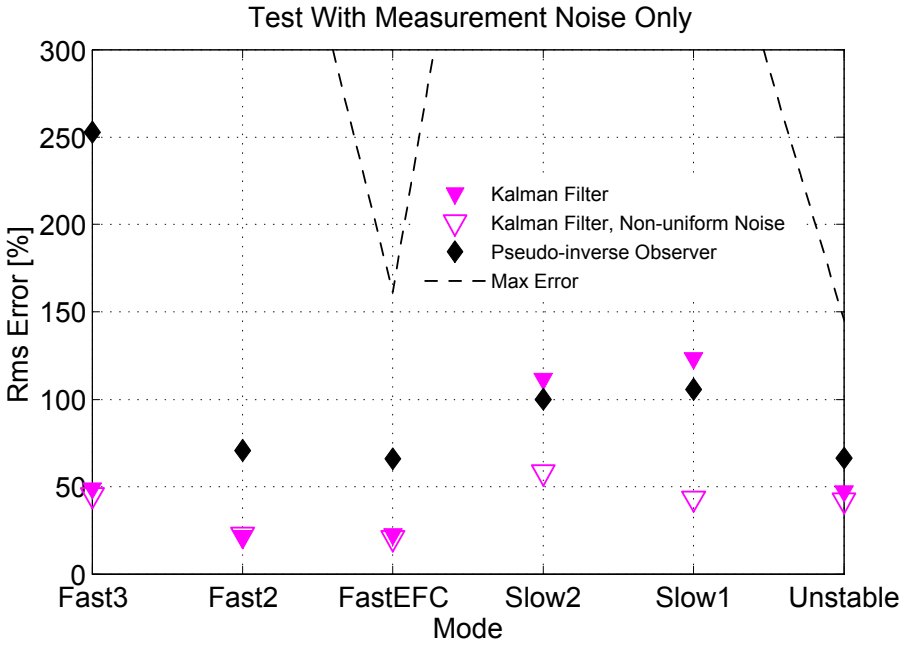

Figure 7: RMS value of the error signals between real and reconstructed states. The $54Hz$ pick-up is off. Results are shown with both uniform ($\alpha^2 = 4$, full triangles) and non-uniform ($\boldsymbol{\alpha}^2 = [4, 4, 4, 64, 64, 4]$, empty triangles) process noise models. Heavier filtering of the slow modes improves overall performance, without compromising their low-frequency signal content.

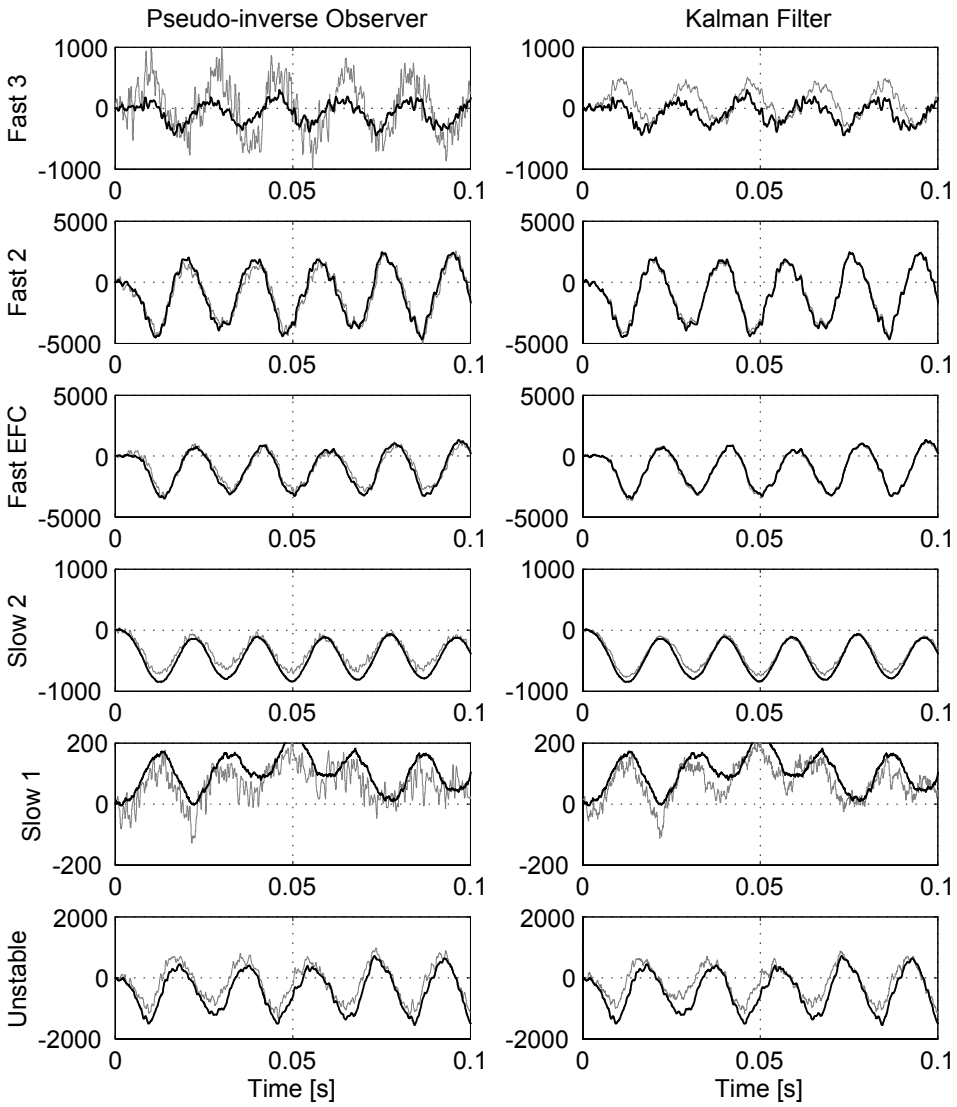

Figure 8: Comparison of real (black) and reconstructed states (light gray). Vertical axes are Amperes. The $54Hz$ pick-up is on. The process noise model is non-uniform with $\boldsymbol{\alpha}^2 = [4, 4, 4, 64, 64, 4]$.

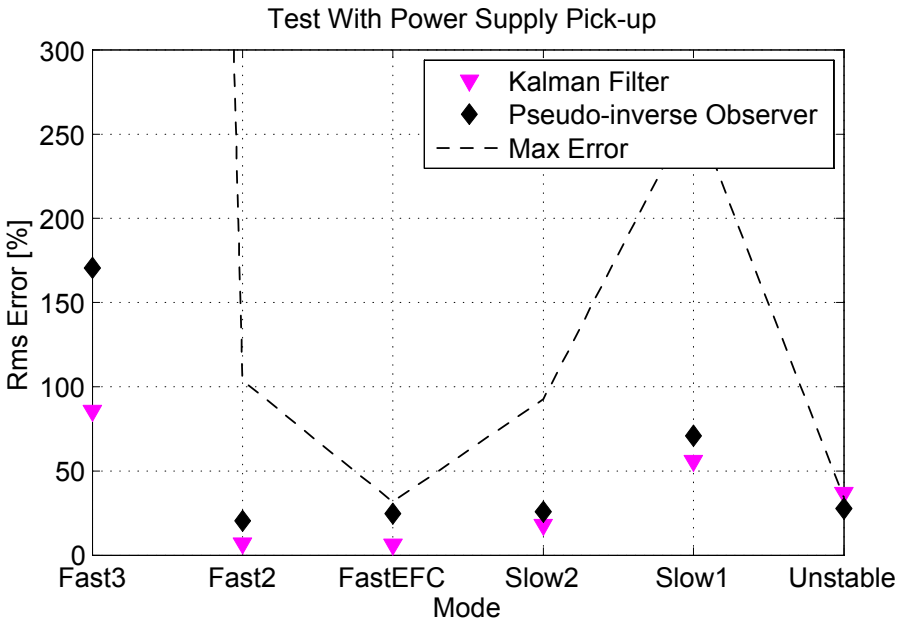

Figure 9: RMS value of the error signals between real and reconstructed states. The $54Hz$ pick-up is on. The process noise model is non-uniform with $\boldsymbol{\alpha}^2 = [4, 4, 4, 64, 64, 4]$.

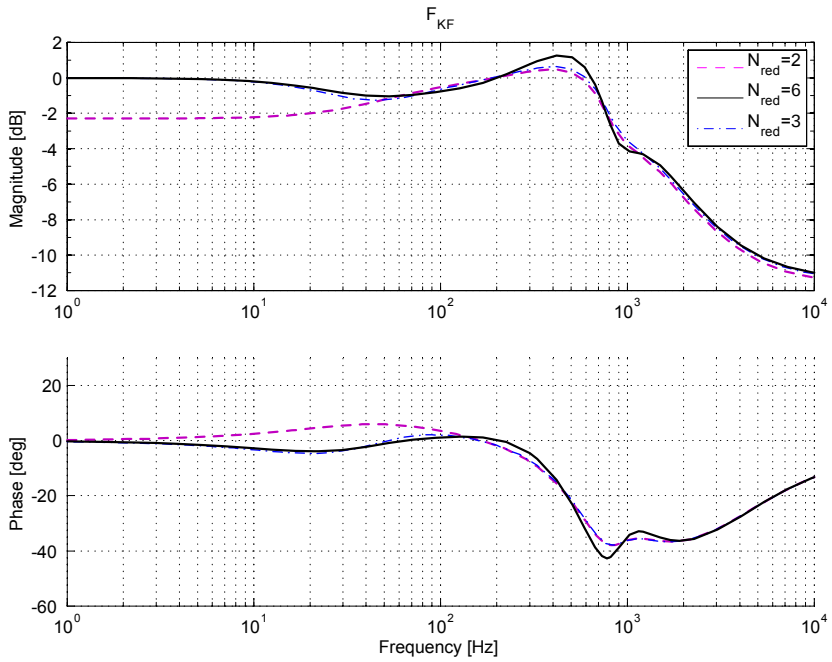

Figure 10: Frequency response of the filter for different orders of the reduced model. For $N_{red} \geq 3$ the slow modes are included and the frequency response has a unitary DC gain, For $N_{red} \geq 6$ the frequency response is practically unchanged. In this example $D = 6$, $P = 4$, $\alpha^2 = 4$.

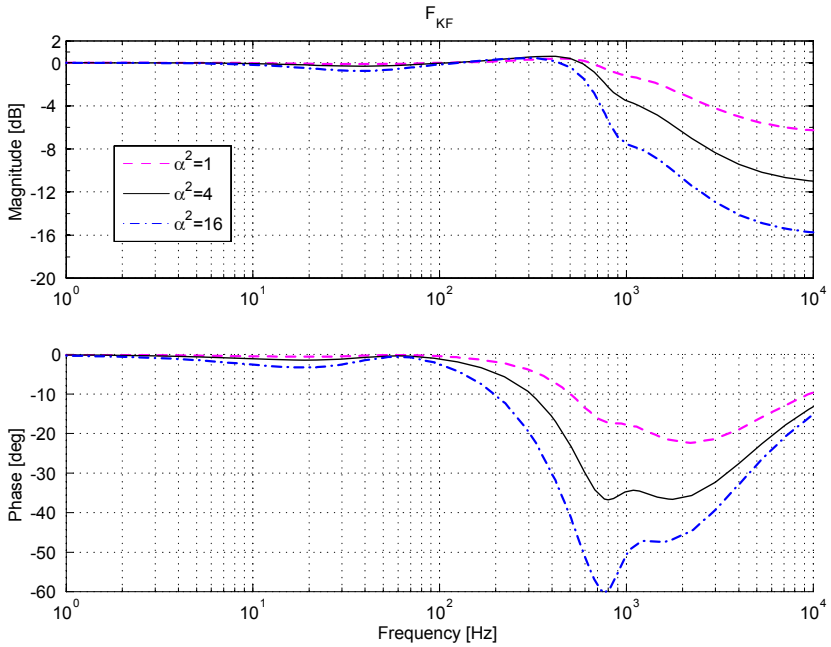

Figure 11: Analytic transfer function of the filter for different values of the noise ratio α^2. High-frequency attenuation is stronger at larger values of α^2.

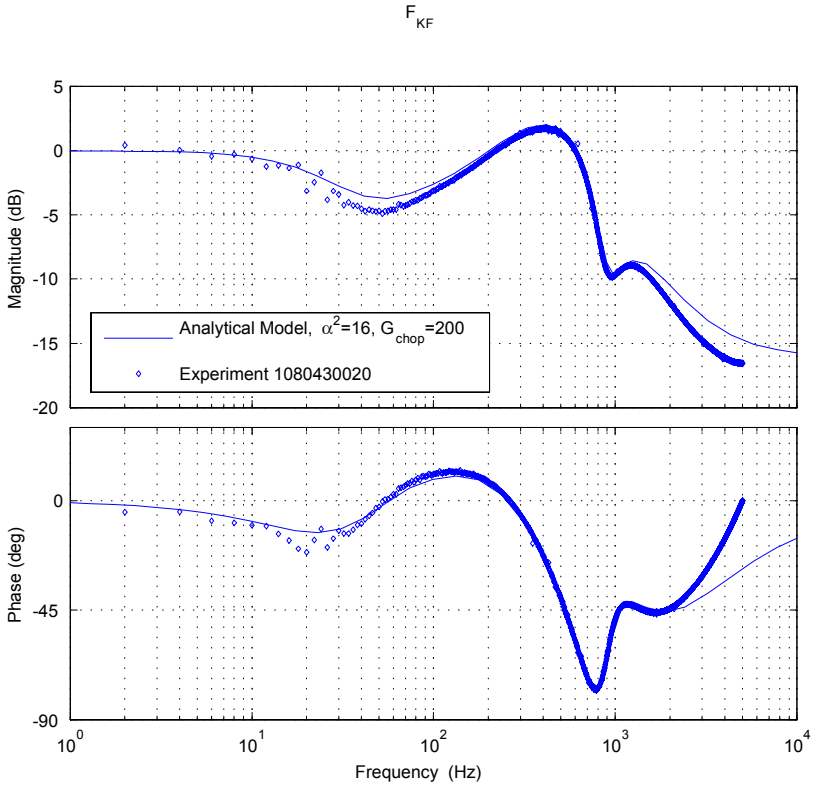

Figure 12: Comparison of analytic and experimental transfer functions. Diamonds are experimental results from a plasma shot, where the filter was operating off-line. The noise ratio was set to a large value $\alpha^2 = 16$. The difference at high frequency is due to the Nyquist cut-off of the experimental digital data, which is not modeled in the analytic transfer function.

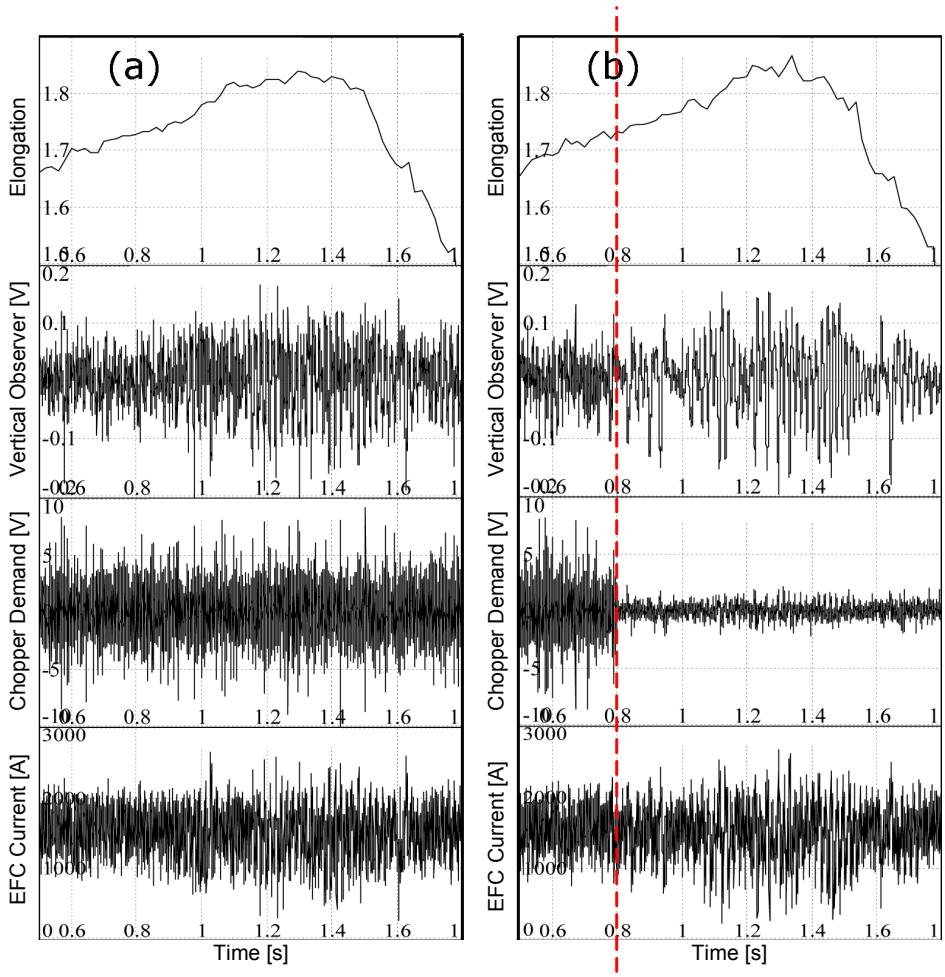

Figure 13: Comparison of two plasma discharges, with the Kalman filter and without. Panels (a) show the plasma elongation, the vertical observer, the chopper demand and the chopper current without the filter, panels (b) show the same quantities with the filter applied after $0.8s$ (dashed line). The elongation is ramped during the discharges. The ripple starting at $1s$, when the elongation peaks, is real plasma motion, with amplitude $5mm$ in physical units.

List of Figures